Optimized ZT of Bi_{2}Te_{3}-GeTe compounds from first principles guided by homogeneous data

Jae Nyeong Kim, Massoud Kaviany, and Ji-Hoon Shim

Phys. Rev. B **93**, 075119 — Published 9 February 2016

DOI: 10.1103/PhysRevB.93.075119

Optimized *ZT* of Bi_2Te_3-GeTe compounds from first-principles guided by homogeneous data

Jae Nyeong Kim,[1] Massoud Kaviany,[2,4] and Ji-Hoon Shim[1,3,4,·]

[1] Department of Chemistry, Pohang University of Science and Technology, Pohang 37673, Korea
[2] Department of Mechanical Engineering, University of Michigan, Ann Arbor, Michigan 48109-2125, USA
[3] Department of Physics, Pohang University of Science and Technology, Pohang 37673, Korea
[4] Division of Advanced Nuclear Engineering, Pohang University of Science and Technology, Pohang 37673, Korea

ABSTRACT

We predict the thermoelectric properties of layered $[GeTe]_m[Bi_2Te_3]_n$ (GBT) compounds ($1 \leq m \leq 8$, $1 \leq n \leq 3$), using first-principles-Boltzmann transport calculations of the homogeneous (Bi_2Te_3 and GeTe) data. The lattice strain and the quantum-confinement effects of compounds evolve the bandgap structures, resulting in asymmetric and large Seebeck coefficient, at high GeTe content. Using semi-empirical calculations of electron scattering rate $1/\tau_e$, dominated by electron-acoustic phonon scattering, we reproduce reported TE properties of GBT compounds. We predict that due to small Seebeck coefficient, the GBT compounds with high *n*- and *p*-type doping ($\sim 10^{20}$ cm^{-3}), do not have high *ZT* near room temperature. However, we predict that the moderately-doped ($\sim 10^{19}$ cm^{-3}), *p*-type GBT compounds have enhanced $ZT \approx 1.4$ near room temperature.

· E-mail: jhshim@postech.ac.kr Phone: +82-54-279-2344 FAX: +82-54-279-3399

I. INTRODUCTION

The layer mixing of heterostructure is promising for enhancing thermoelectric (TE) properties, i.e., the figure of merit $ZT = S^2\sigma T/\rho\kappa$, where S is the Seebeck coefficient, σ is the electrical conductivity, κ is the thermal conductivity, and T is the absolute temperature [1-9]. Intrinsic interface effect modifies the electrical properties by altering the band structures and the bandgap energy. Also the phonon scattering at the interface reduces the lattice thermal conductivity (κ_l), which can dominate κ.

The $[GeTe]_m[Bi_2Te_3]_n$ (GBT) compounds, Fig. 1, are naturally mixed-layer compounds of two distinct TE materials GeTe and Bi_2Te_3 [10-15], having the same rhombohedral symmetry (space group *R3m*, 160). So, GBT compounds with (m, n) can be synthesized, and these as well as the GeTe-Sb_2Te_3 (GST) compounds have also been used in the phase-change memory devices due to their amorphous to cubic/rhombohedral crystal phase transition upon thermal annealing [16-18]. There have been studies on their TE properties with ZT of 0.2 ~ 0.5 at room temperature [12-15,19]. Recently, $[GeTe]_{0.95}[Bi_2Te_3]_{0.05}$ and $[Ge_{0.87}Pb_{0.13}Te]_{0.97}[Bi_2Te_3]_{0.03}$ have been reported with high ZT of 1.6 and 2.0, respectively, so the mixture of the two compounds could also be considered promising [20,21]. The GBT nano-wires were synthesized at various compositions, showing reduced dimensionality and electrical anisotropy enhance TE properties [22]. Theoretically, PbTe-Bi_2Te_3 (PBT) compounds have been predicted to have larger bandgap energy than Bi_2Te_3 and improved TE properties with intermediate operating temperatures [23]. Other theoretical studies of these compounds have been focused on their topological properties [24-27].

Here we investigate the electronic structures and TE properties GBT compounds, using density functional theory (DFT) [28,29] and the Boltzmann transport equations (BTE) [30]. We explore GBT compositions ($1 \le m \le 8$, $1 \le n \le 3$) over a range of temperature 100~500 K. There have been few studies with controlled carrier concentration in GBT compounds [12,19], so consider two representative carrier concentrations: 10^{19} cm^{-3} and 4×10^{20} cm^{-3}. By employing a semi-empirical presentation of electron scattering time (τ_e), we first successfully reproduce the reported ZT of

Bi_2Te_3 and several GBT compounds. Then we proceed to new compounds and predict that their room temperature *ZT* can reach upto 1.4 for $m = 8$ and $n = 1$.

II. METHODS

We used Vienna *ab initio* simulation package (VASP) code for finding optimal crystal structure (both lattice constants and atomic positions) of homogeneous GBT compounds in the range of $1 \leq m \leq 8$ and $1 \leq n \leq 3$ [28]. In the DFT calculation, the projector augmented wave (PAW) method was used with the generalized gradient approximation by Perdew, Burke, and Ernzerhof (PBE-GGA) as an exchange correlation potential [31]. The cut-off energy in the plane-wave expansion of the valence states was set to 500 eV, and the self-consistent-field convergence thresholds were 10^{-4} eV and 0.001 eV/Å for the total electronic energy and force, respectively. The Γ-centered $8\times8\times2$ *k*-mesh was used in the full Brillouin zone (BZ). To treat heavy Bi atoms, we have considered the spin-orbit (SO) coupling. To consider van der Waals (vdW) interaction, we also have considered the Grimme method (DFT-D2).[32] For empirical C_6 and R_0 parameters of Ge and Te, we followed those reported [32] and used C_6 = 63.55 J-nm^6/mol and R_0 = 1.9 Å for Bi [33].

Based on the relaxed crystal structures, we calculate the electronic structure of GBT compounds by using WIEN2k code [29], which uses a full potential linearized augmented plane-wave+local orbitals (L/APW+lo) methods based on the DFT. For the estimation of the band gap, we have tested both PBE-GGA and EV-GGA (GGA by Engel and Vosko) [34] for the exchange correlation potential and found that two results give similar trends, so we only show the results using the PBE-GGA. As the non-overlapping radius of muffin-tin (RMT), 2.5 in atomic unit were used for all atomic species. The $10\times10\times10$ *k*-mesh is used for the self-consistent charge density calculation and dense $36\times36\times36$ *k*-mesh is used for precise description of the TE properties. Using the calculated electronic structures and rigid band approach, the TE properties are calculated with semi-classical BTE implemented in BoltzTraP code [30]. In the BTE, we consider the temperature dependent τ_e with semi-empirical treatment which will be described in Section III.C.

III. RESULTS AND DISCUSSION

A. Crystal and electronic structures

The crystal structures of homogeneous GBT compounds are summarized in Fig. 1 [10,11,15]. According to the reports by Kooi and De Hosson, GeTe is inserted in the middle of Bi_2Te_3 quintuple layers as shown in Fig. 1(c) [35]. For higher compositions of Bi_2Te_3 ($m < n$), GBT compounds have mixed layers with one $GeBi_2Te_4$ and (n-1) Bi_2Te_3 layers as shown in Fig. 1(b). In order to verify the tendency of the lattice parameters with various compositions of GeTe and Bi_2Te_3, we have relaxed all the crystal structures and compared them to the experimental reports. The calculated lattice constants of GBT in Fig. 2(a) show good agreement with the experimental values within 2 % error. This is coming from the choice of vdW interaction, where typical PBE highly overestimate the lattice constants and vdW bond length.[36-39] The lattice constant a and c decrease linearly with the alloying ratio $(m+2n)/(m+3n)$. Figure 2(b) also shows the change of the interlayer distances for each atomic species, which indicates little change of the interlayer distances for a covalent Ge-Te and Bi-Te bonds. So the electronic structure of GBT compounds would be mainly affected by the change of lattice constant a. Note that there are clear differences in the Ge-Te interlayer distances between the GBT compounds and pure GeTe. In pure GeTe, the ferroelectricity makes the distortion in Ge-Te interlayer distances [40]. In the GBT compounds, however, the distortion in Ge-Te interlayer distances is much reduced and it becomes almost cubic like structure. Because cubic GeTe has been suggested as a thermoelectric material with large value of ZT [41], the GBT can be considered mixture of good TE materials, as will be discussed later.

We calculated the electronic structures, using relaxed crystal structures and Fig. 3 shows the orbital projected density of states (DOS), band structures along z direction (cross plane) and bandgap energy ($E_{e,g}$) of the GBT compounds. The $E_{e,g}$ for Bi_2Te_3 is 0.13 eV, comparable to experiment (~ 0.16 eV) [42]. The $E_{e,g}$ for GeTe is 0.34 eV, comparable to experiments (rhombohedral, 0.38 ~ 0.66 eV) [43-45]. For the GBT compounds, Ge and Bi p-orbitals significantly contribute to the

conduction band edge of the bandgap. The Te (1) at the center of Bi_2Te_3 quintuple layer [Fig. 1(a)] contributes to the valence band edge, while Te (2) in the vdW layers contributes to both conduction and valence band edges. The DOS and the band structures of $GeBi_2Te_4$ (m = 1, n = 1) in Fig. 3(b) are similar to those of Bi_2Te_3 in Fig. 3(a), as compared to those of GeTe in Fig. 3(c). The arrows and dashed lines in Fig. 3 indicate band shifts. The bandwidth of Bi_2Te_3 (GeTe) enlarges (shrinks) with respect to their conduction and valence band centers, due to the strain (tensile) in the in-plane lattice constant. Therefore, the bands with Bi_2Te_3 (GeTe) contribution shifts toward (away from) the bandgap center. In Figure S1, the DOS changes for the entire GBT compounds [46], becoming progressively larger with higher GeTe content. In addition to shift in peaks, additional bands with Ge *s*-orbital contribution at the valence band (~ -0.3 eV) become dominant at high GeTe content. The combination of strain and appearance of the Ge *s*-orbital causes asymmetry in DOS (heavier for valence band) at high GeTe content (Fig. S1). This results in asymmetric Seebeck coefficient, with shift toward the conduction band. For moderate doping conditions where the chemical potential is located near the band gap, the Seebeck coefficient for the *p*-type GBT compounds increases, but for the *n*-type it decreases (with sign change).

Another feature in the electronic structures of GBT compounds is the change of dimensionality due to the quantum confinement effect on Bi_2Te_3, where the insertion of GeTe insulating layer separates the Bi_2Te_3 layers. The conduction band minimum and valence band maximum of GBT compounds have mainly Bi_2Te_3 characters near Γ-Z symmetry line. So, the quantum confinement effect reduces the band dispersion near the band gap with increasing GeTe ratio as shown in Fig. 3(d). According to the Mott formula [47], this flat band dispersion results in high Seebeck coefficient along out-of-plane direction for high GeTe content as will be discussed in Section III.C. With the combination of the strain effect and the quantum confinement effect, the obtained $E_{e,g}$s of whole GBT compounds are lower than that of Bi_2Te_3, as summarized in Fig 3(e). The GST compounds with the rhombohedral phase are reported to have almost zero bandgap [48], which is also consistent with our results. It is interesting that Bi_2Te_3, $GeBi_2Te_4$ (m = 1, n = 1), and $Ge_2Bi_2Te_5$ (m = 2, n = 1) behave as topological insulator because of the band gap inversion induced by the strong SO interaction in Bi

atoms [24-27]. As the band dispersion becomes flatter, however, the band gap inversion disappears beyond $Ge_3Bi_2Te_6$ (m = 3, n = 1), which results in minimum $E_{e,g}$, and GBT compounds with higher GeTe content become normal insulators.

B. Semi-empirical approach of electron scattering time

For the calculation of electrical conductivity within the usual BTE calculation, a constant scattering time approximation (CSTA) is used because the exact description of τ_e is challenging due to its multiple mechanisms.[30] The Seebeck coefficients for various TE materials are well reproduced using the BTE with the CSTA [30,49-53], since the constant τ_e cancels out in the calculation steps. However, the electrical conductivity in the BTE only considers the group velocities of the electrons (effective mass) and their thermal activation (carrier concentration) from the bands structures. Figure S2 shows the electrical conductivity tensor ($\Sigma_{e,\mathrm{BTE}}$) from the BTE with the CSTA, for several GBT compounds and Bi_2Te_3. Compared to the experimental electrical conductivity in Figs. S3(a) and (b), there is weak temperature dependence. The complex scattering mechanisms such as electron-phonon scattering, electron-impurity scattering, and point-defect scattering, result in temperature dependence of the electrical conductivity, cannot be realistically included in the CSTA. Therefore, an accurate description of the temperature- and doping-dependent τ_e is critical in predicting the electrical conductivity [54,55]. There have been many attempts to determine each scattering parameters from the first-principles calculations within density perturbation functional theory (DFPT) [56] or by the empirical Kane model considering non-parabolic band dispersion fitted by experimental data [57,58]. However, the DFPT calculations cannot consider the entire scattering mechanisms and the Kane model requires many complicated fitting parameters.

We employed a semi-empirical approach to describe τ_e from the electrical conductivity tensor from the BTE ($\Sigma_{e,\mathrm{BTE}}(T,\mu)$) and the experimental conductivity ($\sigma_{e,exp}(T)$) [12,59-64].

$$\tau_e(T,\mu) = \sigma_{e,exp}(T,\mu)/\Sigma_{e,\mathrm{BTE}}(T,\mu), \qquad (1)$$

where $\Sigma_{e,\mathrm{BTE}}(T,\mu)$ is the directional average of the electrical conductivity tensor $\Sigma_{e,\alpha\beta}(T,\mu)$, given by

$$\Sigma_{e,\alpha\beta}(T,\mu) = \frac{1}{V}\int \Sigma_{e,\alpha\beta}(\varepsilon)\left\{-\frac{\partial f_\mu(T;\varepsilon)}{\partial \varepsilon}\right\} d\varepsilon, \qquad (2)$$

$$\Sigma_{e,\alpha\beta}(\varepsilon) \equiv \sigma_{e,\alpha\beta}(\varepsilon)/\tau_e = \frac{1}{N}\sum_{i,\boldsymbol{k}} e^2 v_\alpha(i,\boldsymbol{k}) v_\beta(i,\boldsymbol{k}) \delta\left(\varepsilon - \varepsilon_{i,\boldsymbol{k}}\right), \qquad (3)$$

where *i* describes the band index, $\boldsymbol{k}$ describes the momentum in Brillouin zone, and Greek letter (α, β) describes directional index. *V* is the volume of unit cell, *N* is the number of $\boldsymbol{k}$-points sampled, $v_\alpha(i,\boldsymbol{k})$ is the group velocity of electron ($= 1/\hbar \cdot \nabla_{\boldsymbol{k}}\varepsilon_{i,\boldsymbol{k}}$), and $f_\mu(T;\varepsilon)$ is Fermi-Dirac distribution at temperature *T* with chemical potential μ. Here, we assume constant τ_e for given momentum and band index, but consider its variation with *T* and μ. Then we estimate $\tau_e(T,\mu)$ with experimental conductivities and the conductivity tensor from the first-principles calculations, for various compounds.

The predicted $\tau_e(T,\mu)$ is compared with experimental results for Bi_2Te_3 and GBT compounds, and summarized in Fig. S3 [46]. For Bi_2Te_3 of moderate carrier density (~10^{19} cm^{-3}), τ_e^{-1} are similar and consistent with the empirical Kane model [58]. The averaged τ_e^{-1} for Bi_2Te_3 shown in Fig. S3(e) is consistent with experiments [59-64], and follows $\sim T^{2.5}$ representing the two-phonon processes in electron-acoustic phonon scattering of non-degenerate semiconductors [54,65]. For the GBT compounds of high carrier density (> 2×10^{20} cm^{-3}), τ_e^{-1} has a behavior expected from the measured conductivity. Here, we use $\tau_e^{-1} = \tau_r^{-1} + AT$, where τ_r^{-1} represents the residual scattering rate and *T* is based on the electron-acoustic phonon scattering for highly degenerate semiconductors. The scatter in τ_r^{-1}, arises from the sample quality (impurity, defect, etc.). So, we choose τ_r^{-1} to give consistent electrical conductivity at room temperature for the GBT compounds [15]. We expect the scattering rate to be nearly the same for the GBT compounds and Bi_2Te_3, for a given carrier density, due to the similar crystal and the band structures. We use the electron scattering time of the Bi_2Te_3 at

10^{19} cm^{-3} (Fig. 4) for the entire GBT compounds at the same doping, and the scattering time of the GBT compounds at 4×10^{20} cm^{-3} for Bi_2Te_3 at the same doping (Fig. 5).

C. TE properties

GBT compounds have naturally high carrier concentration in nature due to the non-stoichiometry of both GeTe and Bi_2Te_3 parts. GeTe is usually highly doped *p*-type material ($p > 2\times10^{20}$ cm^{-3}) with excess Te [66], while Bi_2Te_3 is *n*-type with excess Bi [67]. So, the GBT compounds become *p*-type for high GeTe content ($m > n$) and *n*-type for high Bi_2Te_3 content ($m < n$).[10] Based on the DFT band structures, we have calculated the temperature-dependent TE properties (electrical conductivity, Seebeck coefficient, and *ZT*) of compounds at both hole and electron doping of 10^{19} cm^{-3} and 4×10^{20} cm^{-3}, using the BTE with the semi-empirical description of the scattering time as described above. Note that we only compare the TE properties of Bi_2Te_3 and GBT compounds because the GeTe has a different crystal structure from that of the GeTe in GBT (which results in different electronic structure, as we discussed [41,68]).

Based on the calculated τ_e [inset in Figs. 4(a) and 5 (a)], the experimental electrical conductivities (Figs. 4 and 5) are well reproduced at both moderate (10^{19} cm^{-3}) [61,63,64] and high carrier concentration (4×10^{20} cm^{-3}) [13,14,69]. Note that all the GBT compounds are well described with the same scattering rate, which indicates that the scattering mechanism should be similar between each compounds at given carrier concentration. Since we have assumed the same carrier concentration and residual scattering time τ_r for all compounds, the small disagreement with experimental data can be acceptable. At high carrier concentrations shown in Figs. 4(a) and (b), the electrical conductivities show almost similar results for all GBT compounds and Bi_2Te_3, since they have similar electronic structures at high chemical potential. While, the *n*-type Bi_2Te_3 has higher conductivity due to larger group velocity with more dispersive conduction bands as shown in Fig. 3(d). At moderate carrier concentration shown in Figs. 5(a) and (b), the electrical conductivities of GBT compounds generally show lower values than those of Bi_2Te_3, due to their flatter band

structures near the bandgap [Fig. 3(d)]. For the case of *p*-type GBT, the increased contribution of the Ge *s*-orbital at high GeTe content results in high conductivity close to that of Bi_2Te_3. For the *n*-type cases, there are no such states and the electrical conductivities decrease monotonically as the GeTe content increases.

For the Seebeck coefficient, our results are consistent with experiments from GBT compounds, presented in Figs. 4 and 5, at room temperature. Here, the *n*-type GBT compounds show larger Seebeck coefficient compared to experiments, understandable since the experiments are restricted to large Bi_2Te_3 contents. In Figs. S4, the temperature dependence is also well predicted by our BTE treatment. At high carrier densities, the chemical potential is high enough ($\pm$0.3~0.5 eV) and the Seebeck coefficient is affected by the DOS peak. The Seebeck coefficient of GBT compounds is higher compared to Bi_2Te_3, due to more pronounced DOS peak shifted toward the bandgap. Compared to the *p*-type compounds, the *n*-type shows larger Seebeck coefficient (larger and sharper DOS peak at conduction band). For moderate carrier concentration, the strain and the quantum confinement effects (Section III.A), results in asymmetry and large Seebeck coefficient of the *p*-type GBT compounds at high GeTe contents. However, the *n*-type GBT compounds have smaller Seebeck coefficient (and sign change with temperature).

To calculate *ZT,* we have used the constant lattice thermal conductivities (κ_l) whose values are comparable to the experimental values near 300 K: 1.2 W/m-K for Bi_2Te_3 [63] and 0.5 W/m-K for whole GBT compounds [14]. Also, the electrical thermal conductivity is calculated using the Wiedermann-Franz law [70]. At high carrier concentration shown in Fig. 4, small electrical conductivity and Seebeck coefficients results in small *ZT* of GBT compounds. Despite of small band gap, whole compounds show the enhancement of *ZT* with increasing temperature, which is the characteristic of highly degenerated semiconductor. At moderate carrier concentration shown in Fig. 5, the *p*-type GBT compounds show better TE performances than Bi_2Te_3 with a combination of larger Seebecck coefficient and lower lattice thermal conductivity, while retaining comparable

electrical conductivity. Among the considered compounds, $Ge_8Bi_2Te_{11}$ (m = 8, n = 1) is predicted to have the best TE performances with ZT ~ 1.4.

To check the validity of our results, we have compared our calculated ZT with experimental reports, as summarized in Fig. 6. Here, we have chosen experimental results for the optimal ZT at moderate carrier concentration and room temperature ZT values at high carrier concentration. To show the possible ZT ranges near room temperature, we have plotted the calculated ZT at various temperature ranges (200 ~ 400 K). For moderate carrier concentration, there are few experimental results supporting our calculations, but all showing good agreement. Our results show that the band engineering by lattice-strain and quantum-confinement effect on GBT compounds can enhance the ZT of the p-type Bi_2Te_3 upto 1.4. We expect changing Bi_2Te_3 to $(Bi_{1-x}Sb_x)_2Te_3$, which has higher ZT (~ 1.5) [71], can further enhance the ZT. Note that this carrier density regime may not be optimal for the best thermoelectric performance because the data on scattering properties as function of temperature are available only for two conditions (10^{19} and 4×10^{20} cm^{-3}) given by Fig. S3. At high doping, the calculated ZT shows good agreement with experimental results. The discrepancy in variation of ZT with composition can be due to the residual resistivity of the GBT compounds. All GBT show enhanced ZT at room temperature, compared to pure GeTe. The obtained ZT is similar to that of the cubic $Ge_{1-x}Pb_xTe$ with Bi_2Te_3 doping, which shows high ZT (~ 1.9) at 800 K [21]. Although the electronic structures of GBT compounds and GeTe are much different, it shows that high-dopant GBT compounds could be used in TE devices in the intermediate temperature range.

VI. CONCLUSIONS

In summary, we have checked the electronic structure and TE properties of GBT compounds for various compositions ($1 \leq m \leq 8$, $1 \leq n \leq 3$). GBT compounds are the mixture of GeTe and Bi_2Te_3, where GeTe intercalated in to Bi_2Te_3 quintuple layers. The band structures of GBT compounds are similar to that of Bi_2Te_3 with in-plane strain effect. Also, the separation of Bi_2Te_3 quintuple layers with a large band gap semiconductor GeTe makes for significant quantum-confinement effect on the electronic structures of Bi_2Te_3. With the combination of these two effects, the electronic structures of the GBT compounds have asymmetric distribution of DOS and flat band dispersion near the band gap. On the basis of the electronic structures, we have explored the temperature-dependent TE performance, using semi-empirical electron scattering time. Our results show good agreement with the reported experimental results for high carrier concentration (4×10^{20} cm^{-3}) [13,14]. It shows enhancement of *ZT* over the pure GeTe, considered as good TE material in the intermediate-temperature range [21]. For moderate carrier concentration (10^{19} cm^{-3}), which is optimal doping for Bi_2Te_3 [59-64], the *p*-type GBT with $m = 8$, $n = 1$ is predicted to have best *ZT* upto 1.4 near room temperature. The results show that band engineering by strain and quantum-confinement effect could enhance the TE performances. Also, our semi-empirical τ_e can be used to guide search optimal composition for to other TE systems.

ACKNOWLEDGEMENT

We thank Prof. Jeunghee Park for useful discussion. This research was supported by Global Frontier Program through the Global Frontier Hybrid Interface Materials (GFHIM) of the National Research Foundation of Korea (NRF) funded by the Ministry of Science, ICT & Future Planning (2013M3A6B1078870). M.K. is grateful for support from the US National Science Foundation program on Thermal Transport and Processes (Award No. CBET1332807).

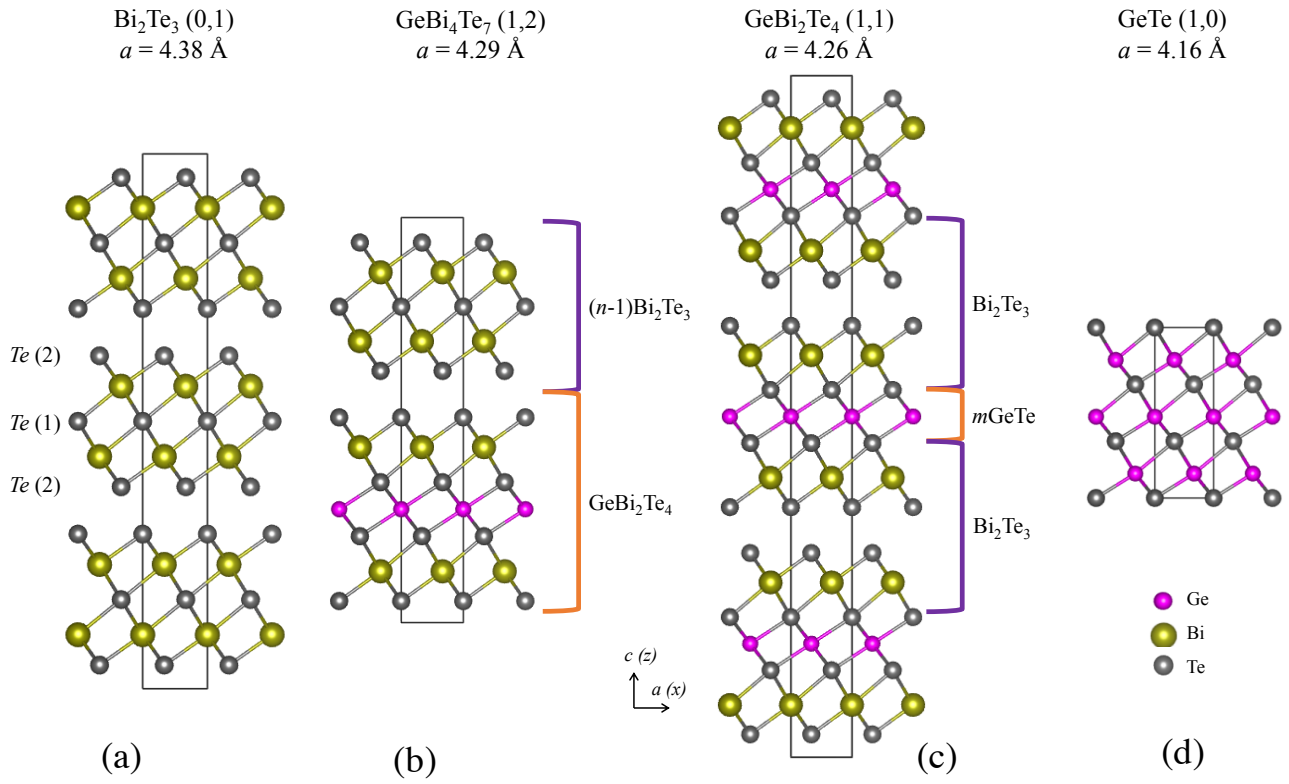

Figure 1 (Color online) Side view of crystal structures for GBT compounds with (*m*, *n*) compositions of GeTe and Bi_2Te_3, guided by the lattice constant *a*. Each color describes Ge (purple), Bi (yellow), and Te (gray) atoms. The crystal structures is obtained by VESTA program.[72]

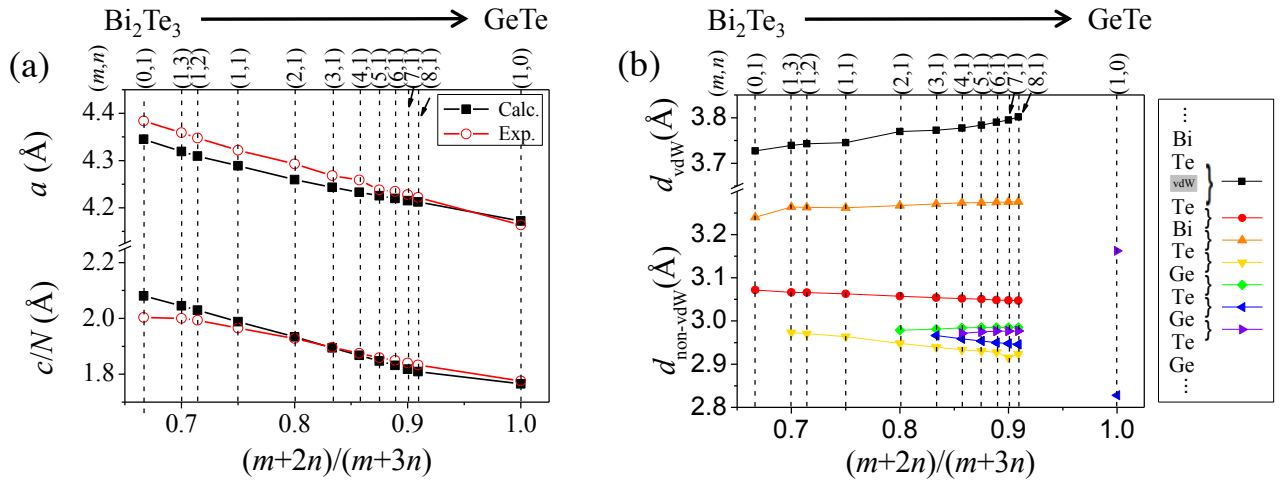

Figure 2 (Color online) (a) Lattice parameters *a* and *c*/*N* (*N*: # of atoms in unit cell) as a function of the alloying ratio (*m*+2*n*)/(*m*+3*n*) which increases with high GeTe content.[10,14] The grid lines indicate the (*m*, *n*) compositions of GeTe and Bi_2Te_3. (b) Inter-layer distances for each atomic layers. The GBT have 2*m*+5 layers in the unit cell and *m* kind of interlayer distances. Each color describes interlayer distances from the vdW layers of gray color (Te-Te) to innermost atomic layers (Te-Ge or Ge-Te).

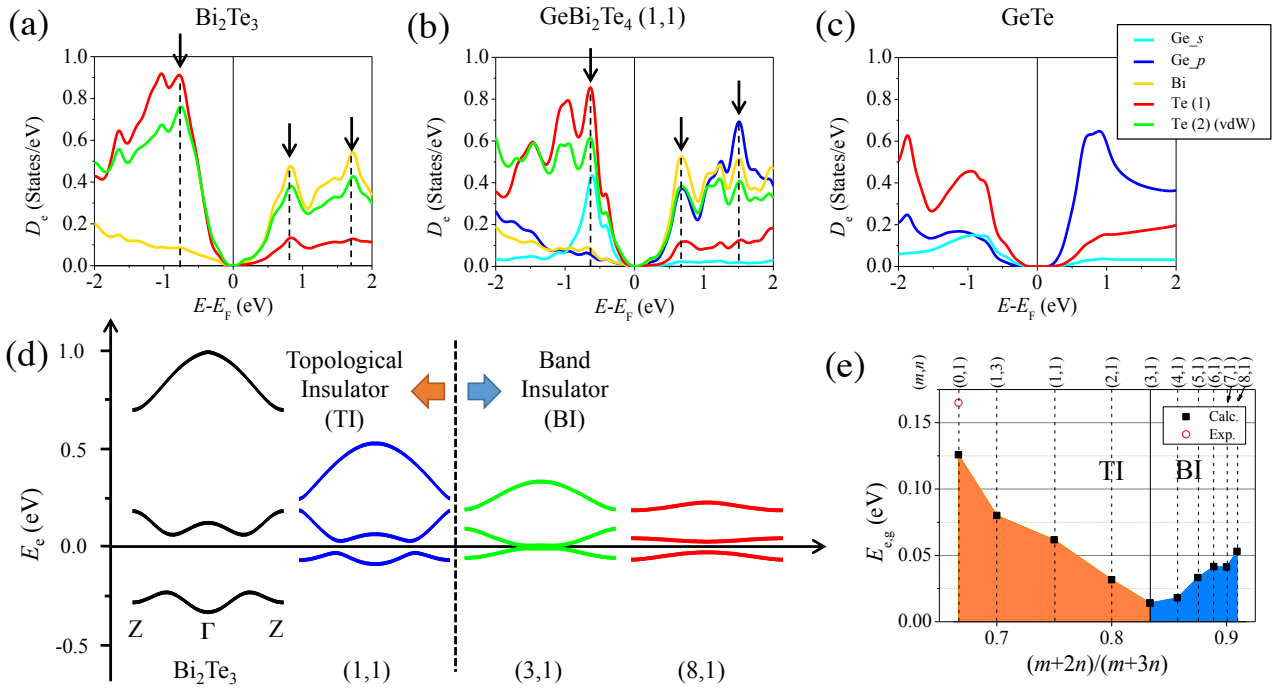

Figure 3 (Color online) (a ~ c) The DOS of Bi_2Te_3, $GeBi_2Te_4$ [(1, 1) composition], and GeTe with their orbital characteristics. The displacement of DOS peaks with similar orbital characteristics are indicated by arrows and dashed lines in the plot. (d) The variations in the band dispersion of Bi_2Te_3 and GBT along the *z*-direction (cross-plane) with composition. (e) Calculated bandgap energy of Bi_2Te_3 and the GBT compounds and comparison with experiments. Each color distinguishes the characteristics of the bandgap as topological insulator and band insulator. See Fig. S1 for the variations of DOS and the band dispersion along the *z*-direction of entire GBT compositions.

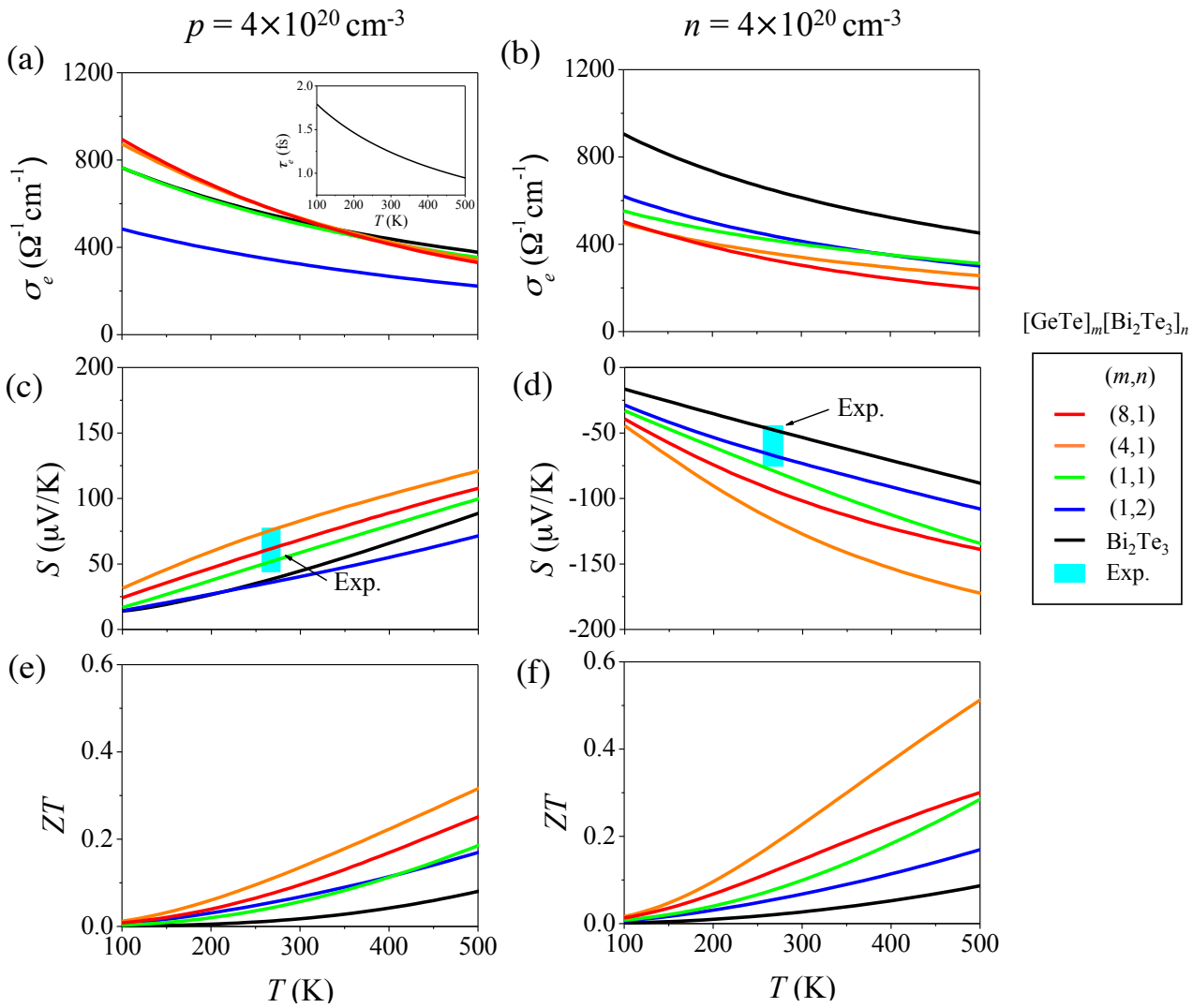

Figure 4 (Color online) The calculated temperature-dependent (a, b) electrical conductivities, (c, d) Seebeck coefficient, and (e, f) *ZT* of the GBT compounds at doping $p(n) = 4\times10^{20}$ cm^{-3}, compared to those of Bi_2Te_3. Inset: The calculated τ_e from Eq. (1).[46]

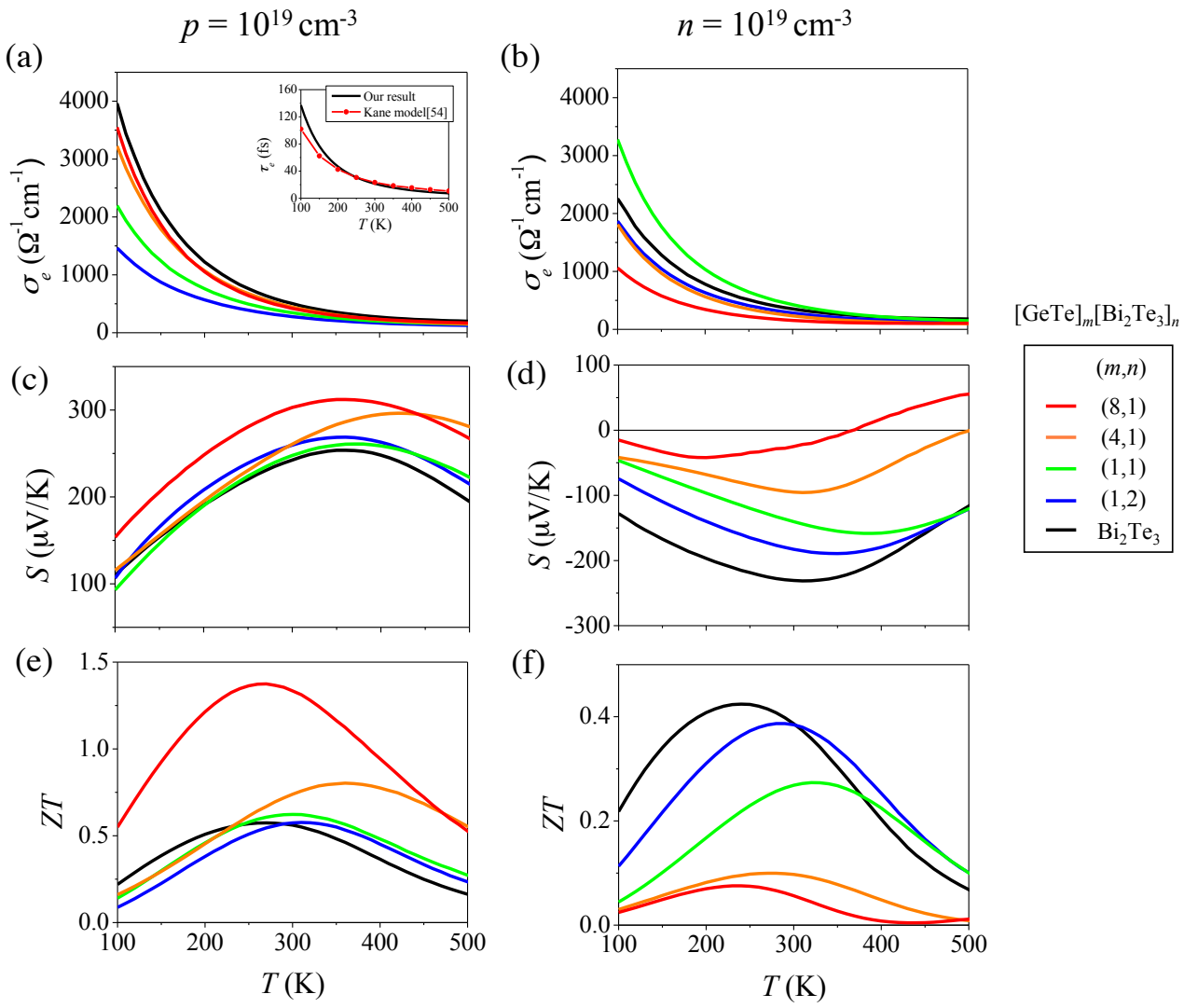

Figure 5 (Color online) The calculated temperature-dependent (a, b) electrical conductivities, (c, d) Seebeck coefficient, and (e, f) ZT the GBT compounds at moderate carrier concentration $p(n) = 10^{19}$ cm^{-3}, compared to those of Bi_2Te_3 Inset: The calculated $\boldsymbol{\tau_e}$ from Eq. (1).[46] It is compared to other reports with the Kane model.[58]

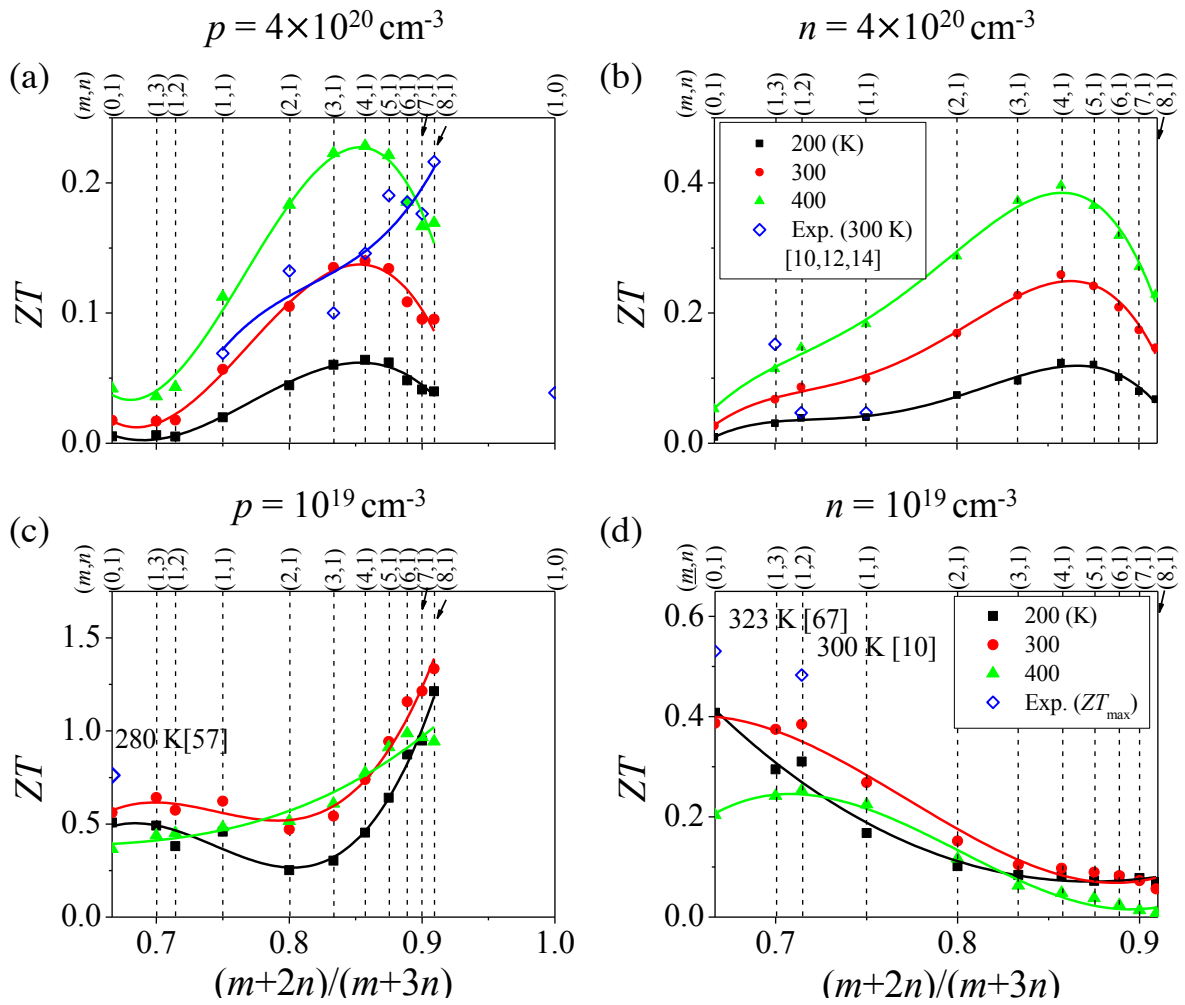

Figure 6 (Color online) Comparison of calculated *ZT* with experiments for Bi_2Te_3[61,73] and the GBT compounds[10,12,14] as a function of composition $(m+2n)/(m+3n)$. For high carrier concentration $p(n) = 4\times 10^{20}$ cm^{-3} (a, b), we have chosen experimental *ZT* at room temperature. For moderate carrier concentration $p(n) = 10^{19}$ cm^{-3} (c, d), we have chosen experimental data of optimal *ZT* for each plot.

REFERENCES

[1] I. Terasaki, Y. Sasago, and K. Uchinokura, Phys. Rev. B. **56**, R12685 (1997).
[2] M. G. Kanatzidis, Acc. Chem. Res. **38**, 359 (2004).
[3] O. G. Karpinskii, L. E. Shelimova, M. A. Kretova, E. S. Avilov, and V. S. Zemskov, Inorg. Mater. **39**, 240 (2003).
[4] L. E. Shelimova, O. G. Karpinskii, T. E. Svechnikova, E. S. Avilov, M. A. Kretova, and V. S. Zemskov, Inorg. Mater. **40**, 1264 (2004).
[5] N. Chen, F. Gascoin, G. J. Snyder, E. Müller, G. Karpinski, and C. Stiewe, Appl. Phys. Lett. **87** (2005).
[6] B. A. Cook, M. J. Kramer, X. Wei, J. L. Harringa, and E. M. Levin, J. Appl. Phys. **101** (2007).
[7] L. D. Zhao, D. Berardan, Y. L. Pei, C. Byl, L. Pinsard-Gaudart, and N. Dragoe, Appl. Phys. Lett. **97** (2010).
[8] S. P. Li, J. Q. Li, Q. B. Wang, L. Wang, F. S. Liu, and W. Q. Ao, Solid State Sci. **13**, 399 (2011).
[9] C. Lee, J. Hong, M.-H. Whangbo, and J. H. Shim, Chem. Mater. **25**, 3745 (2013).
[10] L. E. Shelimova, O. G. Karpinsky, M. A. Kretova, E. S. Avilov, and J. P. Fleurial, in *16th Int. Conf. Thermoelectrics*1997), pp. 481.
[11] O. G. Karpinsky, L. E. Shelimova, M. A. Kretova, and J. P. Fleurial, J. Alloys Compd. **265**, 170 (1998).
[12] P. P. Konstantinov, L. E. Shelimova, E. S. Avilov, M. A. Kretova, and J. P. Fleurial, J. Solid State Chem. **146**, 305 (1999).
[13] L. E. Shelimova, P. P. Konstantinov, O. G. Karpinsky, E. S. Avilov, M. A. Kretova, and J. P. Fleurial, in *Thermoelectrics, 1999. Eighteenth International Conference on*1999), pp. 536.
[14] L. E. Shelimova, P. P. Konstantinov, O. G. Karpinsky, E. S. Avilov, M. A. Kretova, and V. S. Zemskov, J. Alloys Compd. **329**, 50 (2001).
[15] L. E. Shelimova, O. G. Karpinskii, P. P. Konstantinov, E. S. Avilov, M. A. Kretova, and V. S. Zemskov, Inorg. Mater. **40**, 451 (2004).
[16] N. Yamada, E. Ohno, K. Nishiuchi, N. Akahira, and M. Takao, J. Appl. Phys. **69**, 2849 (1991).
[17] C. W. Sun, M. S. Youm, and Y. T. Kim, J. Phys.: Condens. Matter **19**, 446004 (2007).
[18] M. Wuttig and N. Yamada, Nat. Mater. **6**, 824 (2007).
[19] L. E. Shelimova, O. G. Karpinskii, P. P. Konstantinov, M. A. Kretova, E. S. Avilov, and V. S. Zemskov, Inorg. Mater. **38**, 790 (2002).
[20] L. Weintraub, J. Davidow, J. Tunbridge, R. Dixon, M. J. Reece, H. Ning, I. Agote, and Y. Gelbstein, J. Nanomater. **2014**, 7, 284634 (2014).
[21] D. Wu, L.-D. Zhao, S. Hao, Q. Jiang, F. Zheng, J. W. Doak, H. Wu, H. Chi, Y. Gelbstein, C. Uher, C. Wolverton, M. Kanatzidis, and J. He, J. Am. Chem. Soc. **136**, 11412 (2014).
[22] C. S. Jung, H. S. Kim, H. S. Im, K. Park, J. Park, J. P. Ahn, S. J. Yoo, J. G. Kim, J. N. Kim, and J. H. Shim, Nano Lett. **15**, 3923 (2015).
[23] L. Zhang and D. J. Singh, Phys. Rev. B. **81**, 245119 (2010).
[24] T. V. Menshchikova, S. V. Eremeev, Y. M. Koroteev, V. M. Kuznetsov, and E. V. Chulkov, Jetp Lett. **93**, 15 (2011).
[25] J. Kim, J. Kim, K.-S. Kim, and S.-H. Jhi, Phys. Rev. Lett. **109**, 146601 (2012).
[26] M. Neupane, S. Y. Xu, L. A. Wray, A. Petersen, R. Shankar, N. Alidoust, C. Liu, A. Fedorov, H. Ji, J. M. Allred, Y. S. Hor, T. R. Chang, H. T. Jeng, H. Lin, A. Bansil, R. J. Cava, and M. Z. Hasan, Phys. Rev. B. **85**, 235406 (2012).
[27] S. V. Eremeev, G. Landolt, T. V. Menshchikova, B. Slomski, Y. M. Koroteev, Z. S. Aliev, M. B. Babanly, J. Henk, A. Ernst, L. Patthey, A. Eich, A. A. Khajetoorians, J. Hagemeister, O. Pietzsch, J. Wiebe, R. Wiesendanger, P. M. Echenique, S. S. Tsirkin, I. R. Amiraslanov, J. H. Dil, and E. V. Chulkov, Nat. Commun. **3**, 635 (2012).
[28] G. Kresse and J. Furthmüller, Phys. Rev. B. **54**, 11169 (1996).

[29] P. Blaha, K. Schwarz, G. Madsen, D. Kvasnicka, and J. Luitz, WIEN2K, An Augmented Plane Wave + Local Orbitals program for calculating crystal properties, 2001.
[30] G. K. H. Madsen and D. J. Singh, Comput. Phys. Commun. **175**, 67 (2006).
[31] J. P. Perdew, K. Burke, and M. Ernzerhof, Phys. Rev. Lett. **77**, 3865 (1996).
[32] S. Grimme, J. Comput. Chem. **27**, 1787 (2006).
[33] A. T. Clay, C. M. Kuntz, K. E. Johnson, and A. L. L. East, J. Chem. Phys. **136** (2012).
[34] E. Engel and S. H. Vosko, Phys. Rev. B. **47**, 13164 (1993).
[35] B. J. Kooi and J. T. M. De Hosson, J. Appl. Phys. **92**, 3584 (2002).
[36] X. Luo, M. B. Sullivan, and S. Y. Quek, Phys. Rev. B. **86**, 184111 (2012).
[37] V. L. Deringer and R. Dronskowski, The Journal of Physical Chemistry C **117**, 15075 (2013).
[38] L. Cheng, H. J. Liu, J. Zhang, J. Wei, J. H. Liang, J. Shi, and X. F. Tang, Phys. Rev. B. **90**, 085118 (2014).
[39] B.-T. Wang, P. Souvatzis, O. Eriksson, and P. Zhang, J. Chem. Phys. **142**, 174702 (2015).
[40] A. I. Lebedev, I. A. Sluchinskaya, V. N. Demin, and I. H. Munro, Phase Transitions **60**, 67 (1997).
[41] X. Chen, D. Parker, and D. J. Singh, Sci. Rep. **3** (2013).
[42] R. Sehr and L. R. Testardi, J. Phys. Chem. Solids **23**, 1219 (1962).
[43] S. Yamanaka, S. Ogawa, I. Morimoto, and Y. Ueshima, Jpn. J. Appl. Phys. **37**, 3327 (1998).
[44] J.-W. Park, S. H. Eom, H. Lee, J. L. F. Da Silva, Y.-S. Kang, T.-Y. Lee, and Y. H. Khang, Phys. Rev. B. **80**, 115209 (2009).
[45] D. J. Singh, J. Appl. Phys. **113**, 203101 (2013).
[46] *See Supplementary Material at [link] for the change of DOS with varying GeTe & Bi_2Te_3 compositions, the electrical conductivity tensor from the BTE with the CSTA, the information for τ_e, and the comparision between the calculated Seebeck coefficients to experimental one.*
[47] M. S. Dresselhaus, G. Chen, M. Y. Tang, R. G. Yang, H. Lee, D. Z. Wang, Z. F. Ren, J. P. Fleurial, and P. Gogna, Adv. Mater. **19**, 1043 (2007).
[48] D. Subramaniam, C. Pauly, M. Liebmann, M. Woda, P. Rausch, P. Merkelbach, M. Wuttig, and M. Morgenstern, Appl. Phys. Lett. **95** (2009).
[49] G. K. H. Madsen, J. Am. Chem. Soc. **128**, 12140 (2006).
[50] J.-S. Rhyee, K. H. Lee, S. M. Lee, E. Cho, S. I. Kim, E. Lee, Y. S. Kwon, J. H. Shim, and G. Kotliar, Nature **459**, 965 (2009).
[51] C. Sevik and T. Çağın, Appl. Phys. Lett. **95**, 112105 (2009).
[52] D. J. Singh, Phys. Rev. B. **81**, 195217 (2010).
[53] J. M. Tomczak, K. Haule, and G. Kotliar, Proc. Natl. Acad. Sci. **109**, 3243 (2012).
[54] B. M. Askerov, *Electron transport phenomena in semiconductors* (World Scientific, 1994), Vol. 394.
[55] N. W. Ashcroft and N. D. Mermin, *Solid state physics* (Holt, Rinehart and Winston, New York, 1976).
[56] J. Sjakste, N. Vast, and V. Tyuterev, Phys. Rev. Lett. **99**, 236405 (2007).
[57] E. O. Kane, J. Phys. Chem. Solids **1**, 249 (1957).
[58] B.-L. Huang and M. Kaviany, Phys. Rev. B. **77**, 125209 (2008).
[59] H. J. Goldsmid, Proc. Phys. Soc. London, Sec. B **69**, 203 (1956).
[60] S. Shigetomi and S. Mori, J. Phys. Soc. Jpn. **11**, 915 (1956).
[61] H.-W. Jeon, H.-P. Ha, D.-B. Hyun, and J.-D. Shim, J. Phys. Chem. Solids **52**, 579 (1991).
[62] L. Jansa, P. Lošťák, J. Šrámková, and J. Horák, J. Mater. Sci. **27**, 6062 (1992).
[63] L. D. Ivanova and Y. V. Granatkina, Inorg. Mater. **36**, 672 (2000).
[64] V. A. Kulbachinskii, V. G. Kytin, A. A. Kudryashov, and P. M. Tarasov, J. Solid State Chem. **193**, 47 (2012).
[65] E. Z. Gershtein, T. S. Stavitskaya, and S. b. L.S., Soviet Phys. Tech. Phys. **2**, 2302 (1957).
[66] K. L. Chopra and S. K. Bahl, J. Appl. Phys. **40**, 4171 (1969).
[67] C. B. Satterthwaite and R. W. Ure, Jr., Phys. Rev. **108**, 1164 (1957).
[68] L. Xu, H.-Q. Wang, and J.-C. Zheng, J. Electron. Mater. **40**, 641 (2011).

[69] S. Bäßler, T. Böhnert, J. Gooth, C. Schumacher, E. Pippel, and K. Nielsch, Nanotechnology **24**, 495402 (2013).
[70] R. Franz and G. Wiedemann, Annalen der Physik und Chemie **165**, 497 (1853).
[71] W. Xie, X. Tang, Y. Yan, Q. Zhang, and T. M. Tritt, Appl. Phys. Lett. **94**, 102111 (2009).
[72] K. Momma and F. Izumi, J. Appl. Crystallogr. **44**, 1272 (2011).
[73] L.-D. Zhao, B.-P. Zhang, W.-S. Liu, and J.-F. Li, J. Appl. Phys. **105**, 023704 (2009).